A MINIATURE PHOSWICH DETECTOR FOR GAMMA-RAY LOCALIZATION AND BETA IMAGING

Martin P. Tornai*, *Member, IEEE*, Craig S. Levin, *Member, IEEE*, Lawrence R. MacDonald, *Member, IEEE*, Clay H. Holdsworth, and Edward J. Hoffman, *Senior Member, IEEE*

Division of Nuclear Medicine & Biophysics, Department of Molecular & Medical Pharmacology, UCLA School of Medicine, Los Angeles, CA 90095

ABSTRACT

A combined γ-ray probe/$\beta^{\pm}$ imaging detector was created by modification of a beta imaging intra-operative probe. This phoswich detector consists of a thin $CaF_2(Eu)$ $\beta^{\pm}$ imaging disk, coupled through a light diffuser to 7 or 19 parallelepiped high-Z scintillation crystals arranged hexagonally in columns. These elements are either 2x2x10 mm^3 or 4x4x10 mm^3 LSO, GSO or BGO crystals, and act as both light guides for the imaging light and as intrinsic γ detectors. The coincidence between the $CaF_2(Eu)$ and phoswich scintillators identifies β^+ or true β^- events and suppresses accompanying annihilation or background γ events. The phoswich crystals are in turn coupled through optical fibers to a multi-channel PMT with positioning and discrimination electronics. Various characteristics of this novel imaging phoswich detector are inves-tigated and presented for each of the phoswich combinations including: detector anisotropy, effects of time blocking and energy windows on phoswich imaging, intrinsic singles and phoswich spectral and spatial resolution characteristics, and phoswich imaging ability within γ background environments. The performance characteristics of the assembled prototype devices demonstrate that in surgery, this device can be used three ways: (1) rapid localization of γ emitting radionuclides with the modestly directional, self-collimated phoswich crystals; (2) high resolution β^- imaging or coarse (annihilation background corrupted) β^+ imaging in singles mode; or (3) β^+ imaging in coincidence mode with reduced γ background contamination.

I. INTRODUCTION

More complete tumor resection has been shown to increase the life span and improve the quality of life of surgically treated patients [1,2]. This has been an underlying motivation in our development of beta [2-5] and gamma [2,3,6,7] sensitive imaging detectors. This class of intra-operative imaging detectors is designed to help delineate the remnant tumor boundaries which a surgeon could subsequently remove.

One anticipated high specificity, brain tumor radiotracer (^{18}F-fluorodeoxyuridine) emits positrons (β^+) whose annihilation γ's can also be imaged with PET. Direct β^+ detection with the accompanying 511 keV annihilation γ backgrounds in the patient's body, however, was shown to degrade image contrast [5]. A background count rate of ~1.5 cts/sec/μCi was measured with the $CaF_2(Eu)$ based imaging detector [5], which is approximately 5 times greater than the anticipated β^+ count rate from the exposed, labeled tumor tissue. Thus, it is necessary to reduce or eliminate the γ background contribution for this fiber-coupled, scintillator based imaging detector in order to produce artifact free images of the β^+ distributions.

*Present address: *Duke University Medical Center, Dept. of Radiology, DUMC-3949, Durham, NC 27710*

II. BACKGROUND SUPPRESSION TECHNIQUES

A. Phoswich Detector Configurations

Three techniques were considered to measure γ background contamination when detecting β^+ distributions or for γ background suppression with β^- emitting nuclides with additional γ decay components (Fig. 1). The secondary γ-annular detector (left) was previously investigated, and successfully imaged β^+ distributions in background environments [5]. This configuration, however, has a poor detection efficiency, is somewhat cumbersome and increases the overall size of the imaging detector, which may preclude using the device in small cavities. The second phosphor sandwich technique (middle), or phoswich [8], replaces the necessary light diffuser with a high-Z scintillator providing a large solid angle for detection of annihilation radiation. This technique also suffers from poor detection efficiency due to the required thinness of the light diffuser in order to obtain high spatial resolution from the imaging detector. Thus, the third technique (right) combines the phoswich detector concept into a compact and efficient imaging detector which has a greater probability of detecting γ's with its large volume and solid angle to the imaging detector. Other phoswich imaging devices have used columnar sandwiched phoswich detectors [9-11] but not this combination of imaging disk and columnar secondary (phoswich) detectors.

B. Optical Coupling of the Phoswich Components

High-Z and high density crystals were investigated for the proposed phoswich configuration. The parallelepiped crystals were highly polished on all surfaces. The available crystals were: BGO, each 2x2x10 mm^3; GSO, each 4x4x10 mm^3; LSO, each either 2x2x10 mm^3 or 4x4x10 mm^3.

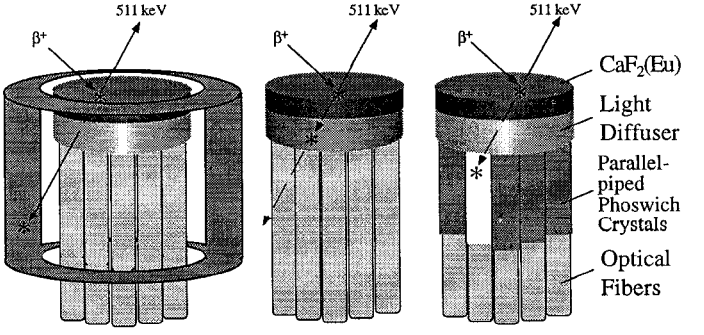

FIGURE 1. Conceptualization of three detection techniques. (Left) The ideal annular, coincident (and independent) detector is bulky. (Middle) Replacing the necessary light diffuser with a phoswich crystal suffers from inefficiency due to the detector thinness required for good spatial resolution from the adjunct imaging detector. (Right) There is a larger interaction probability with the phoswich detectors arranged in a columnar array; they act as both guides for the imaging light and as the phoswich detectors.

0-7803-4258-5/98/$10.00 © 1998 IEEE

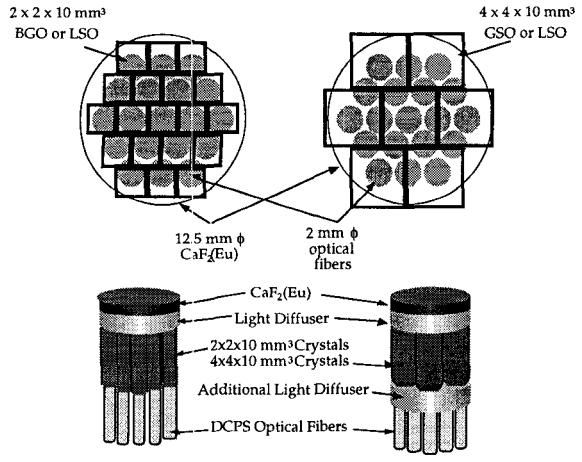

FIGURE 2. Top-down and perspective views of the coupling between the imaging $CaF_2(Eu)$ scintillator, light diffuser, square cross-section phoswich detectors, and round cross-section optical fibers in the hexagonal array.

TABLE 1. Measured decay times and intrinsic spectral resolution at 662 keV, and intrinsic spatial resolution measured with 0.1 mm ^{204}Tl beta slit source with the phoswich combinations.

Characteristic	19 Elements (each 2x2x10 mm³)		7 Elements (each 4x4x10 mm³)	
	LSO	BGO	LSO	GSO
λ (nsec)* (measured (actual))	60 (42)	303 (300)	--	104 (60)
Pulse Height (Mean ± σ %)	100 ± 20.3	19.4 ± 3.6	57.4 ± 11.8	30.5 ± 8.5
%FWHM (Mean ± σ %)	21.1 ± 6.13	65.4 ± 24.0	39.4 ± 5.10	66.0 ± 13.5
%FWHM Range	11.2 - 33.0	38.4 - 100.2	35.9 - 49.8	42.1 - 82.7
X-Resolution (FWHM ± σ mm)	1.09 ± 0.18	1.00 ± 0.04	3.25 ± 0.56	3.51 ± 0.44
Y-Resolution (FWHM ± σ mm)	1.00 ± 0.14	1.33 ± 0.37	--	--

* Values measured from the imaging phoswich detector with the digital oscilloscope.

The 2x2 mm² cross-sections match well with the 2 mm ϕ double clad optical fibers used in the imaging probe [2-6], but the optical coupling was not ideal in these investigations (Fig. 2). Nevertheless, each of the smaller crystals in the array could be moderately well read out by the optical fibers. For the 4x4 mm² cross-section crystals, an additional light diffuser was required in order to form an image of the crystal arrays, similar in concept to the unmatched, discrete crystal light sharing implementation employed with the gamma image probes [6].

III. SIGNAL SEPARABILITY

A. *Preamplifier Time Constant*

The integrals of the various phoswich scintillator preamplifier signals (total light output) were compared to the integral $CaF_2(Eu)$ signal as a function of preamplifier time constant (τ). Not surprisingly, the optimal calculated time constant occurs when the total light output ratio of the phoswich to $CaF_2(Eu)$ signal is maximized, which is near the decay time (λ) of the faster phoswich scintillator ($\tau_{preamplifier} \approx \lambda_{faster}$).

Measurements of the imaging PMT anode signal from the various phoswich combinations were made with τ around the calculated optimal values. Each of the imaging scintillator

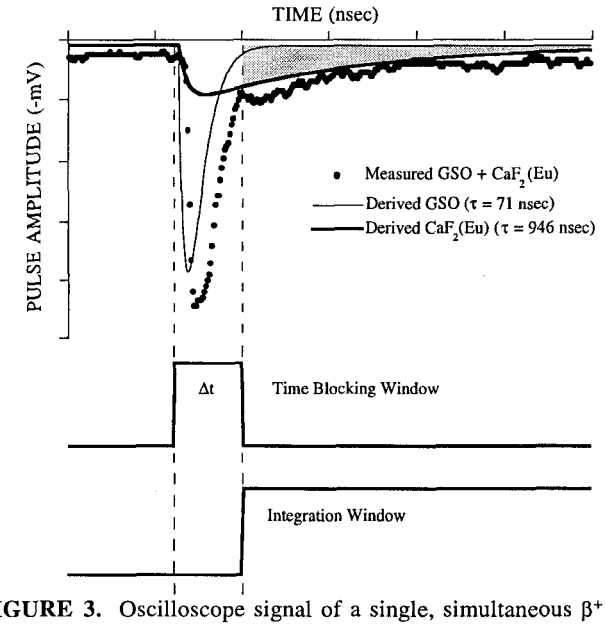

FIGURE 3. Oscilloscope signal of a single, simultaneous β^+ and annihilation γ event measured with the $CaF_2(Eu)$ and GSO phoswich. The smooth curves are derived from parameter estimates from the simultaneous data. The first logic pulse overlaps the majority of the gamma portion of the simultaneous event, and blocks the faster portion of the signal from passing through a NC linear gate. The second logic corresponds in time to the integration window of the imaging portion of the signal.

phoswich combinations (as in Fig. 2) was independently irradiated with either ^{204}Tl (β^- E_{max} = 765 keV) or ^{137}Cs (662 keV γ) to discern the individual signals. The anode signal from the MC-PMT (*Philips* XP1722) (Fig. 4) was fed to a fast filter amplifier (*Ortec* 579) with various τ; the resultant time based pulses were digitized with a LabVIEW™ driven *Tektronix* 2430 digital oscilloscope with GPIB connection to a *Macintosh* IIfx. The λ of the scintillators were extracted by fits to the measurements with the near optimal τ = 50 nsec (Table 1). The measured λ's slightly over or underestimated the known values for the scintillators. This is in part because the measurements were made for a single event, and utilized only the most significant 8 bits in the 16 bit oscilloscope digitizer to minimize noise.

B. *Time Blocking Window*

Simultaneous β^+ + γ events were recorded with a point source of ^{18}F on the $CaF_2(Eu)$ imaging surface with GSO phoswich (Fig. 3, top). The smooth curves in the figure were derived from fits of the double decay time spectrum of the simultaneous event. A coincidence is established between a β^+ and γ event by imposing both an energy threshold and additional time threshold or time blocking window. If the energy threshold is set above the highest measured $CaF_2(Eu)$ only signal, which can be measured with the ^{204}Tl pure β^- source as an analog to the ^{18}F β^+ events, then only two types of events satisfy the energy threshold in the phoswich: (1) single γ events and (2) simultaneous β^+ + γ events.

Given that the energy threshold in a discriminator is satisfied by an event, a time blocking window is triggered, as shown by the first logic pulse in Fig. 3. The blocking window size (Δt) is affected by the combined signal amplitudes. The essential premise of the time blocking window is to screen out or block the non-imaging γ contribution from the

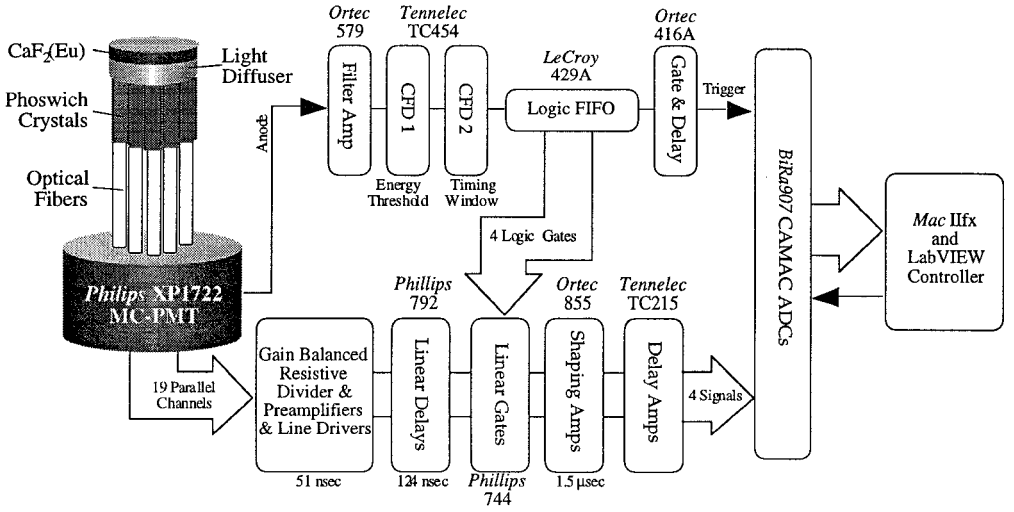

FIGURE 4. Electronic circuit for coincidence phoswich imaging. Detector is on the left. Upper pathway (NIM) provides energy and timing discrimination to validate coincident events; lower pathway (NIM) multiplexes and conditions signals for position decoding.

imaging portion. A NIM linear gate module can be used to block portions of a signal (e.g. Fig. 4). If a signal passes through the linear gate, it will be integrated and shaped, as indicated by the second logic window. This technique is somewhat different than one which utilizes two time-to-digital converters of different time lengths (one short and one longer) to integrate the respective signals [13], but is similar in that two gates of different time duration are utilized to isolate the signal components. Additional spectroscopy information may be obtained when using two charge digitizers with different gate lengths in a phoswich device [9,13]. The longer charge sensitive gate, however, may integrate considerable noise along with the real signal.

C. Electronic Circuit for Phoswich Imaging

The detected MC-PMT signals follow two pathways (Fig. 4). The MC-PMT anode signal combines the signals from the 19 optical fibers, regardless of the gain variations of any individual pixel signal. This is then filtered and linearly amplified before undergoing energy (CFD1) and timing discrimination (CFD2) with two constant fraction discriminators. Provided the anode signal satisfies the energy threshold, the resultant time blocking logic signal is split into four logic gates with the Fan-In-Fan-Out (FIFO) module which triggers a normally closed (NC) linear gate.

The 19 parallel imaging signals are passively gain balanced, resistively divided (multiplexed) and preamplified as shown on the lower pathway. A $\tau = 51$ nsec ($R = 510\ \Omega \pm 5\%$ and $C = 1000$ pF $\pm$ 20%) was used on each of the *Maxim* 410 preamplifiers [2,4]. This value was considered more optimal for LSO and GSO than BGO, in combination with $CaF_2(Eu)$. This is also considerably shorter than the $\tau = 2$ µsec previously reported for the $CaF_2(Eu)$ only, beta imaging probe. This NC linear gate passes all of the signal which does not correspond in time with the blocking window.

IV. RAPID GAMMA LOCALIZATION

A. Energy Resolution Characteristics

The energy spectra and pulse heights for each phoswich crystal (Table 1) were extracted from crystal element look-up

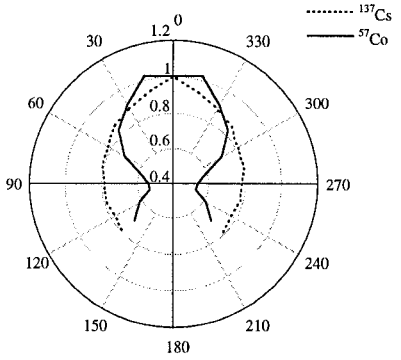

FIGURE 5. Directional anisotropy results for the relative sensitivity of the central crystal in the GSO phoswich irradiated with ^{137}Cs and ^{57}Co from 2.5 cm. Note that with the less penetrating ^{57}Co γ's, the measured anisotropy is enhanced.

tables developed for these unique crystal coupling arrangements, but are similar in concept to those utilized for the discrete gamma imaging probes [6]. The BGO phoswich crystal regions were determined with the 2x2x10 mm^3 element LSO crystals which were identical in size, but more easily distinguishable.

Clearly, the higher light output LSO scintillator had overall better energy resolution and pulse height characteristics than either the BGO or GSO phoswich crystal arrays. However, it is not clear whether superior energy resolution is important in this phoswich application. One reason for the relatively poor energy resolution values is due to the non-optimal optical coupling between the phoswich detectors and optical fibers which conduct the signal to the remotely located MC-PMT (Fig. 2). Intrinsic detector and geometric efficiency are important in order to maintain a good sensitivity for the coincident gamma particles of interest, although detection by means of Compton scatter may be all that is required in order to produce a valid coincidence signal level. Knowledge of the energy resolution parameters are also important as a component to optimizing the threshold and time discrimination settings in the imaging phoswich detectors.

B. Active Collimation for Rapid Localization

Utilizing the phoswich crystals in singles (γ only) mode

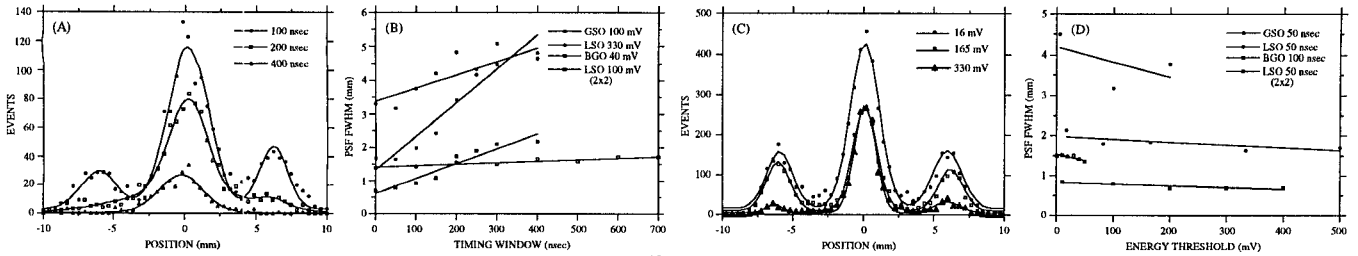

FIGURE 6. Characteristic PSF profiles made with the 1 mm ^{18}F point source and (A) various timing windows for a nominal energy threshold with the GSO phoswich, and (C) various energy thresholds for a 50 nsec fixed timing window with the 4x4x10 mm^3 LSO phoswich. Graphs (B) and (D) include the results for combinations of timing window blocking and energy threshold PSF profiles in (A) and (C), respectively, as well as other phoswich combinations.

adds functionality to the imaging detector. Thus the phoswich crystals could rapidly localize tumor hot spots based on proximity effects determined with count rate measurements. The crystals can be used as a self-collimated non-imaging γ ray detector, where the outer ring(s) of crystal elements act to shield the inner-most element of the phoswich array (Fig. 2). The information from the central most crystal can be digitally extracted. Then, by calculating the number of events in the central most crystal compared to the total number of events collected for a fixed time, an estimate of the "sensitivity" of the central crystal to the source can be made. This solid angle argument relies on the fact that the efficiency of the central most crystal changes with the different exposed area and detection efficiency of the outer rings of phoswich elements. The important parameter is the ratio of counts in the center to the total detected counts, which gives the magnitude of the sensitivity to a point source.

For all phoswich combinations, the anisotropy of the detector sensitivity to sources at various radial and azimuthal locations was measured with ^{137}Cs and ^{57}Co point sources held by a goniometer at fixed distances (2.5, 5 and 10 cm) from the center of the phoswich array and differing by 15° increments. Due to the nature of the square crystals in the phoswich array (Fig. 2), the anisotropy was not expected to be completely rotationally symmetric for all polar angles about the central axis of the phoswich array.

A window was placed over all of the crystal energy spectra, thus only the photopeak events were included in the calculation. While GSO has the lowest Z_{eff} and density of all the phoswich crystals, its sensitivity anisotropy response was the most pronounced (Fig. 5: a 20% effect from normal to a 90° azimuth). The strength of the anisotropy was considerably more pronounced at lower energy, as expected, due to the higher absorption of the γ's in the outer active shield of the crystal array. Thus, not only would this phoswich detector be able to image $\beta^{\pm}$ emissions in various backgrounds, but the device could be used to rapidly locate these lower energy γ sources, as is currently performed with non-imaging γ probes.

V. PHOSWICH IMAGING CHARACTERISTICS

A. Intrinsic Spatial Resolution Performance

The intrinsic, non-coincidence spatial resolution was measured with a 0.1 mm black PMMA slit collimated ^{204}Tl beta source stepped in 1.0 mm increments across the FOV of the various phoswich detector configurations (Table 1). For all cases with the LSO crystals, the natural background caused image artifacts. Thus, a long background acquisition, time normalized to the beta slit source acquisitions was subtracted from the images and yielded a more uniform image in which the line source was more clearly distinguishable. Even with image normalization, hot spots were still apparent in the various images, but LSF profiles could still be measured from the image data.

B. Variation of Energy Thresholds and Blocking Window

Using a 1 mm ϕ ^{18}F source in PMMA, imaging measurements were made with the various phoswich configurations. The effects of the time blocking window width on the measured emission spatial resolution were characterized (Fig. 6A,B). As the length of the time blocking window is increased with a low energy threshold, less of the tail of the γ signal is integrated, suppressing the non-β^+ background (seen as lobes in the PSF profiles). In addition, less of the β^+ imaging signal is integrated, thus the spatial resolution degrades (Fig. 6B). This is also seen as a decreased PSF amplitude.

The cumulative effects of the time blocking window width and energy threshold on the measured emission spatial resolution were also characterized (Fig. 6C,D). As the energy threshold for a given time blocking window is increased, only true $\beta^+ + \gamma$ events satisfy the energy requirement, suppressing γ only events (also seen as lobes in the PSF profiles). This is more effective for the dimmer γ sensitive detectors. In addition, with higher thresholds, higher energy β^+'s are selected (larger positioning pulse height), resulting in somewhat improved spatial resolution. For both the time blocking window and combined time blocking and energy threshold discrimination, the best results are shown, and do not account for the finite source size or inherent β^+ range in the holder or imaging detector.

C. Preliminary Extrinsic Imaging Performance

The CaF_2(Eu)/BGO phoswich was characterized in its ability to image complex β^+ emission distributions (Fig. 7) without and with various γ backgrounds. BGO was used since

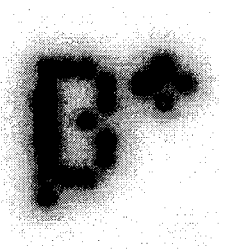

FIGURE 7. High resolution digital autoradiograph (25 μm intrinsic FWHM resolution) of the ^{18}F filled β^+ emission phantom. Total volume is ~4 μL in the 21 element 0.5 mm ϕ wells in PMMA, spaced on 0.6 mm horizontal and vertical pitch.

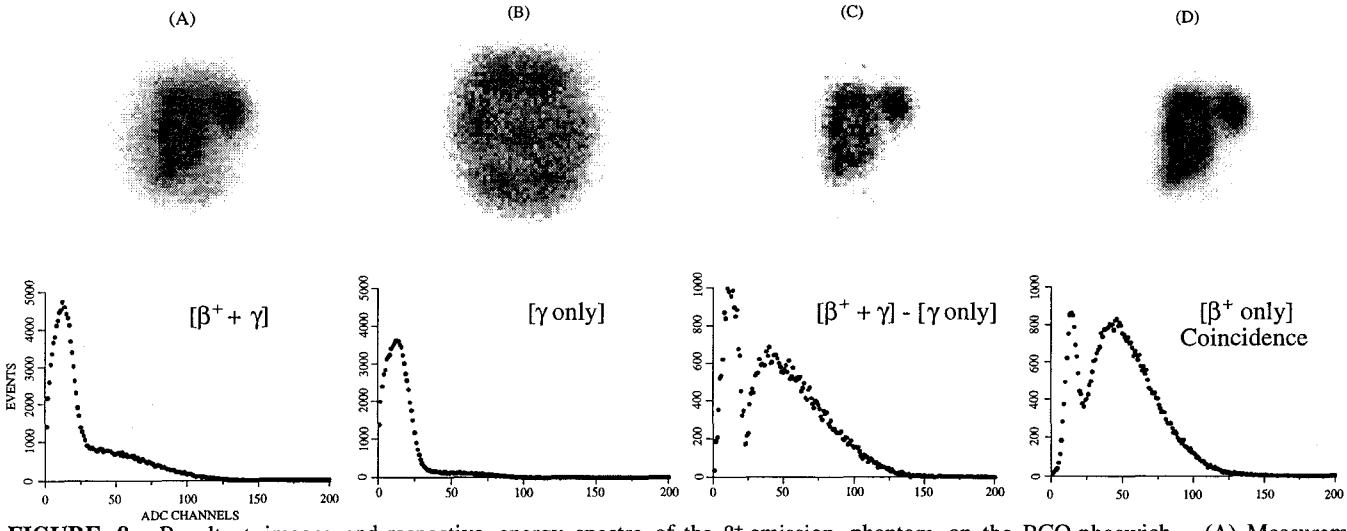

FIGURE 8. Resultant images and respective energy spectra of the β^+ emission phantom on the BGO phoswich. (A) Measurement without any background rejection (no energy or timing thresholds) includes both β^+ and γs; (B) measurement of the γ component by shielding the β^+ with a 0.4 mm thin Cu plate; (C) the difference image and spectrum of (A) - (B); (D) coincidence image with 100 nsec time blocking window and 50 mV threshold. There are ~4x higher statistics in (D) than in (C), and the respective energy spectra were count normalized.

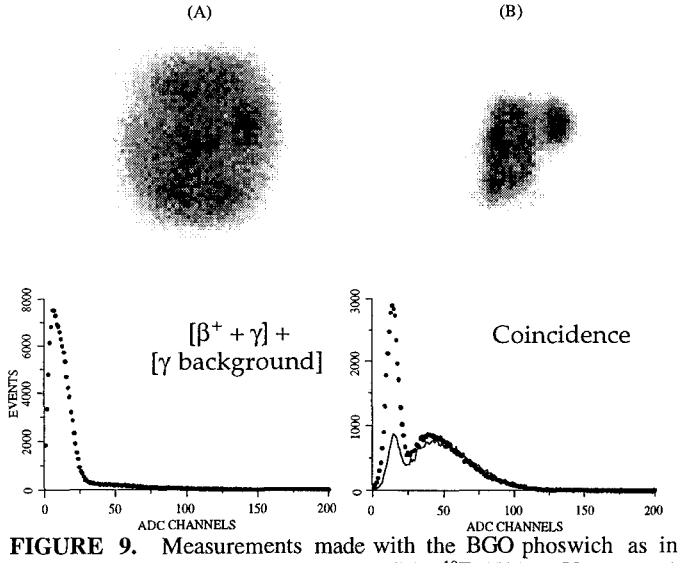

FIGURE 9. Measurements made with the BGO phoswich as in Fig. 8 but with an additional 250 μCi/L ^{18}F (511 keV γ source) activity in 400 mL water directly behind the β^+ emission phantom. Measurements made (A) without and (B) with background rejection with the 50 mV and 100 nsec time blocking thresholds. Spectral data in (B) includes the spectra from Fig. 8D (solid line) to illustrate the increased gamma component in the lower energy portion of the spectrum due to the added γ background.

it demonstrated good spatial resolution characteristics and no intrinsic background signals. A resolution degradation was expected based on the intrinsic resolution values of the original $\beta^{\pm}$ imaging probe [2,4] and measured characteristics of the phoswich probes. Qualitatively, the phoswich imaging results are similar to the difference image (Fig. 8), which is considered a good reference [5]. With the additional γ back-ground activity, the imaging phoswich detector extracted the β^+ signal, with a noticeably increased γ contribution (Fig. 9).

These initial experiments validate the utility and versatility of this novel phoswich imaging probe. Several improvements can be made in the final imaging device, including choice and geometry of scintillator, and improved fiber optic coupling. These devices also need to be tested in more realistic environments to validate their effectiveness for *in situ* use.

ACKNOWLEDGMENTS

The authors thank Drs. S. Cherry and M. Dahlbom for use of the LSO, BGO and GSO crystals, Dr. S. Majewski for helpful discussions, K. Meadors and D. Kim for expert technical assistance, and Dr. G. Clark for the use of his digital oscilloscope. This work was funded in part by NIH/NCI grants R01-CA61037, T32-CA09092, DOE contract DE-FC03-87-ER60615.

REFERENCES

[1] M Ammirati, *et al.* 1987. Effect of the Extent of Surgical Resection on Survival and Quality of Life in Patients with Supratentorial Glioblastomas and Anaplastic Astrocytomas. *Neurosurgery.* **21**(2): 201-206.

[2] MP Tornai. 1997. *Small Area Beta and Gamma Detectors for Functional Nuclear Emission Imaging.* UCLA. Ph.D. Thesis, and references therein.

[3] EJ Hoffman, *et al.* 1997. Gamma and Beta Intra-Operative Probes. *Nucl. Instr. Meth.* **A389**:324-329.

[4] MP Tornai, *et al.* 1996. Design Considerations and Initial Performance of a 1.2 cm^2 Beta Imaging Intra-Operative Probe. *IEEE Trans. Nucl. Sci.* **43**(4):2326-2335.

[5] CS Levin, *et al.* 1997. Annihilation γ Ray Background Characterization and Rejection for a Small Beta Camera Used for Tumor Localization During Surgery. *IEEE Trans. Nucl. Sci.* **44**(3):1120-1126.

[6] MP Tornai, *et al.* 1997. Investigation of Crystal Geometries for Fiber Coupled Gamma Imaging Intra-Operative Probes. *IEEE Trans. Nucl. Sci.* **44**(3):1254-1261.

[7] BE Patt, *et al.* 1997. Development of an Intraoperative Gamma Camera Based on a 256-Pixel Mercuric Iodide Detector Array. *IEEE trans. Nucl. Sci.* **44(3)**:1242-1248.

[8] DH Wilkinson. 1952. The Phoswich - A Multiple Phosphor. *Rev. Sci. Instr.* **23**(8):414-417.

[9] M Bantel, *et al.* 1984. A Two-Dimensional Position Sensitive Phoswich Detector. *Nucl. Instr. Meth.* **226**:394-404.

[10] Z He, D Ramsden. 1993. A Broad-Band Position Sensitive Phoswich Detector for Gamma-Ray Astronomy. *Nucl. Instr. Meth.* **A336**:330-335.

[11] M Dahlbom, *et al.* 1997. Performance of a YSO/LSO Detector Block for Use in a PET/SPECT System. *IEEE Trans. Nucl. Sci.* **44**(3):1114-1119.

[12] GF Knoll. 1979. *Radiation Detection and Measurement.* John Wiley & Sons, Inc. New York.

[13] DA Cebra, WK Wilson. AV Molen, GD Westfall. 1992. The Light Response of Plastic Scintillators and the Calibration of Large Arrays. *Nucl. Instr. Meth.* **A313**:367-372.